

KalmanNet: Neural Network Aided Kalman Filtering for Partially Known Dynamics

Guy Revach, Nir Shlezinger, Xiaoyong Ni, Adrià López Escoriza, Ruud J. G. van Sloun, and Yonina C. Eldar

Abstract—Real-time state estimation of dynamical systems is a fundamental task in signal processing and control. For systems that are well-represented by a fully known linear Gaussian state space (SS) model, the celebrated Kalman filter (KF) is a low complexity optimal solution. However, both linearity of the underlying SS model and accurate knowledge of it are often not encountered in practice. Here, we present KalmanNet, a real-time state estimator that learns from data to carry out Kalman filtering under non-linear dynamics with partial information. By incorporating the structural SS model with a dedicated recurrent neural network module in the flow of the KF, we retain data efficiency and interpretability of the classic algorithm while implicitly learning complex dynamics from data. We numerically demonstrate that KalmanNet overcomes non-linearities and model mismatch, outperforming classic filtering methods operating with both mismatched and accurate domain knowledge.

I. INTRODUCTION

State estimation of dynamical systems in real-time is one of the most fundamental tasks in signal processing and a problem of interest to various scientific communities. In his pioneering work from the 1960s described by a series of papers [2]–[4], Rudolf Kalman introduced the Kalman filter (KF), a minimum mean-squared error (MMSE) estimator that is applicable to time-varying linear systems characterized by a state space (SS) model with additive white Gaussian noise (AWGN). The low-complexity implementation of the KF, combined with its sound theoretical basis, resulted in it quickly becoming the leading work-horse of state estimation in systems that are well described by SS models in discrete-time. The KF has been applied to problems such as radar target tracking [5], trajectory estimation of ballistic missiles [6], and estimating the position and velocity of a space vehicle in the Apollo program [7]. To date, the KF and its variants are still widely used as online filtering algorithms in numerous real world applications involving tracking and localization [8].

While the original KF assumes linear SS models, many problems encountered in practice are governed by non-linear

dynamical equations. Therefore, shortly after the introduction of the original KF, non-linear variations of it were proposed, such as the extended Kalman filter (EKF) [5], and the unscented Kalman filter (UKF) [9]. These variations for non-linear SS models are not theoretically optimal, and suffer from severe degradation in the face of strong non-linearity [10]. The original KF and its variations are *model-based* (MB) algorithms; namely, they rely on accurate knowledge of the underlying SS model. As such, the performance of these MB methods critically depends on the validity of this domain knowledge. In practice, the underlying dynamics are often complex, non-linear, and difficult to accurately estimate and characterize as a tractable SS model.

Recent years have witnessed remarkable empirical success of deep neural networks (DNNs) in real-life applications. These data-driven (DD) parametric models were shown to be able to catch the subtleties of the true generative process and replace the need to explicitly characterize the domain of interest [11], [12]. Therefore, an alternative strategy to implement state estimation—without requiring explicit and accurate knowledge of the SS model—is to learn this task from data using deep learning. DNNs can be trained in an end-to-end model-agnostic manner from a large quantity of data to capture complex dynamics. In particular, various DNN architectures, including recurrent neural networks (RNNs) models such as long short-term memory (LSTM) [13] and gated recurrent unit (GRU) cells [14], as well as attention mechanisms [15], have been shown to learn to carry out time series prediction. While such DD architectures preform very well in unstructured environments, they lack the interpretability of MB methods and tend to require many trainable parameters even for seemingly simple sequence models [16]. These constraints limit the application of highly parametrized deep models for real-time state estimation in applications embedded in hardware-limited mobile devices such as drones and vehicular systems.

The limitations of MB Kalman filtering and DD state estimation motivate a hybrid approach that exploits the best of both worlds; i.e., the soundness and low complexity of the classic KF, and the model-agnostic nature of DNNs. Therefore, we build upon the success of our previous works in MB deep learning for signal processing and digital communication applications [17]–[20], to propose a hybrid MB/DD online recursive filter, coined KalmanNet. In particular, we focus on real-time state estimation for continuous-value SS models for which the KF and its variants are designed. We assume that the noise statistics are unknown, and the underlying SS model is partially known or approximated from a physical

Parts of this work focusing on linear Gaussian state space models were accepted for presentation in the IEEE International Conference on Acoustics, Speech, and Signal Processing (ICASSP) 2021 as the paper [1]. G. Revach, X. Ni and A. L. Escoriza are with the Signal Processing Laboratory (ISI), Department of Information Technology and Electrical Engineering, ETH Zürich, Switzerland (e-mail: grevach@ethz.ch; xiaoni@student.ethz.ch; alopez@student.ethz.ch). N. Shlezinger is with the School of ECE, Ben-Gurion University of the Negev, Beer Sheva, Israel (e-mail: nirshl@bgu.ac.il). R. J. G. van Sloun is with the EE Dpt., Eindhoven University of Technology, and with Phillips Research, Eindhoven, The Netherlands (e-mail: r.j.g.v.sloun@tue.nl). Y. C. Eldar is with the Faculty of Math and CS, Weizmann Institute of Science, Rehovot, Israel (e-mail: yonina.eldar@weizmann.ac.il).

model of the system dynamics. To design KalmanNet, we identify the Kalman gain (KG) computation of the KF as a critical component encapsulating the dependency on the noise statistics and domain knowledge, and replace it by a compact RNN of limited complexity, which is integrated into the KF flow. The resulting system uses labeled data to learn to carry out Kalman filtering in a supervised manner.

Our main contributions are summarized as follows:

- 1) We design KalmanNet, which is an interpretable, low complexity, and data-efficient DNN-aided real-time state estimator. KalmanNet builds upon the flow and theoretical principles of the KF, incorporating partial domain knowledge of the underlying SS model in its operation.
- 2) By learning the KG, KalmanNet circumvents the dependency of the KF on knowledge of the underlying noise statistics, thus bypassing numerically problematic matrix inversions involved in the KF equations, and overcoming the need for tailored solutions for non-linear systems; e.g., approximations to handle non-linearities as in the EKF.
- 3) We show that KalmanNet learns to carry out Kalman filtering from data in a manner that is invariant to the sequence length. Specifically, we present an efficient supervised training scheme that enables KalmanNet to infer on arbitrary long trajectories while only training using short trajectories.
- 4) We evaluate KalmanNet in linear and non-linear SS models. The experimental scenarios include a synthetic setup, tracking the chaotic Lorenz system, and localization using the Michigan NCLT data set [21]. KalmanNet is shown to converge much faster compared with purely DD architectures, while outperforming the MB EKF when facing model mismatch and dominant non-linearities.

The rest of this paper is organized as follows: Section II reviews the SS model and its associated tasks, and discusses related works. Section III details KalmanNet and a discussion. Section IV presents the numerical study. Section V provides concluding remarks and future work.

Throughout the paper, we use boldface lower-case letters for vectors, and boldface upper-case letters for matrices. The transpose, ℓ_2 norm, and stochastic expectation are denoted by $\{\cdot\}^\top$, $\|\cdot\|$, and $\mathbb{E}[\cdot]$, respectively. The Gaussian distribution with mean μ and covariance Σ is denoted by $\mathcal{N}(\mu, \Sigma)$. Finally, \mathbb{R} and \mathbb{Z} are the sets of real and integer numbers, respectively.

II. SYSTEM MODEL AND PRELIMINARIES

A. State Space Model

We consider a (possibly) time-varying dynamical system represented by a non-linear, Gaussian, continuous SS evolution model in discrete-time $t \in \mathbb{Z}$ [22]

$$\begin{aligned} \mathbf{x}_t &= \mathbf{f}(\mathbf{x}_{t-1}) + \mathbf{e}_t, & \mathbf{e}_t &\sim \mathcal{N}(\mathbf{0}, \mathbf{Q}), & \mathbf{x}_t &\in \mathbb{R}^m, & (1a) \\ \mathbf{y}_t &= \mathbf{h}(\mathbf{x}_t) + \mathbf{v}_t, & \mathbf{v}_t &\sim \mathcal{N}(\mathbf{0}, \mathbf{R}), & \mathbf{y}_t &\in \mathbb{R}^n. & (1b) \end{aligned}$$

Here, \mathbf{x}_t is the latent state vector of the system at time t , which evolves by a (possibly) non-linear state evolution function $\mathbf{f}(\cdot)$, and by an AWGN \mathbf{e}_t without a control signal. This SS model is graphically described in Fig. 1 as a factor graph.

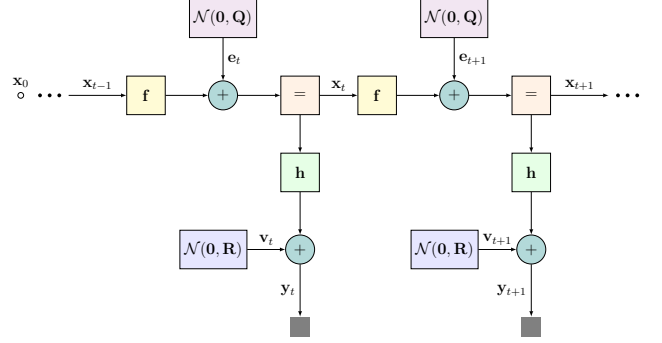


Fig. 1: SS model illustration (factor graph).

The process noise \mathbf{e}_t usually models inaccuracies in the state evolution function and unknown external inputs. The system is partially observable; i.e., the vector of observations \mathbf{y}_t at time t is generated by a (possibly) non-linear function $\mathbf{h}(\cdot)$ from \mathbf{x}_t with AWGN \mathbf{v}_t . In practice, the state evolution model (1a) is determined by the complex dynamics of the underlying system, while the observation model (1b) is dictated by the type and quality of the observations. For instance, \mathbf{x}_t can determine the location, velocity, and acceleration of a vehicle, while \mathbf{y}_t are measurements obtained from several sensors. The parameters of these models—e.g., the covariance matrices \mathbf{Q} and \mathbf{R} —may be difficult to obtain accurately, often leading to performance degradation due to model mismatch.

B. Associated Tasks

SS models are studied in the literature in the context of several different tasks. These tasks can be roughly classified into two main categories: *observation generation* and *denoising*, and *hidden state recovery*.

- The first family of tasks associated with SS models deals with the estimation of parts of the observation signal. This can correspond to, e.g., the prediction of future observations given past observations; the generation of missing observations in a given block via imputation; and the denoising of the observations. While such tasks focus on estimation of the observation signal \mathbf{y}_t , they exploit the presence of an underlying SS model in doing so.
- The second category considers the recovery of the hidden state \mathbf{x}_t of a predefined structure from noisy observations obeying a SS model. The family of state recovery tasks includes offline recovery, also referred to as *smoothing*, where the recovery of the entire block is $\{\mathbf{x}_t\}_{t=1}^T$, given the entire block of observations $\{\mathbf{y}_t\}_{t=1}^T$. Alternatively, the *filtering* task focuses on the recovery of \mathbf{x}_t only from past observations $\{\mathbf{y}_\tau\}_{\tau=1}^t$, corresponding to real-time state estimation.

In this work we focus on the filtering task, where the exact formulation is given in the following subsection.

C. Data-Aided Filtering Problem Formulation

The filtering problem, where one must provide an instantaneous state estimate based on each incoming observation in an online manner, is at the core of real-time tracking. Here, at

each time instance t , we are given access to a new observation \mathbf{y}_t . Given the initial state \mathbf{x}_0 , the goal is to track the current hidden state \mathbf{x}_t and to produce an estimate for it $\hat{\mathbf{x}}_t$.

We focus on scenarios where one has partial knowledge of the system model, namely, we know (or have an approximation of) the evolution function $\mathbf{f}(\cdot)$ and the observation function $\mathbf{h}(\cdot)$. For real world applications, this knowledge is derived from our understating of the system dynamics, its physical design, and the model of the sensors. As opposed to the classical assumptions in KF, the noise statistics \mathbf{Q} and \mathbf{R} are not known. Instead, we have access to a labeled data set containing a sequence of observations and their corresponding ground truth states. In various scenarios of interest one can assume access to some ground truth measurements in the design stage. For example, in field experiments it possible to add extra sensors both internally or externally to collect the ground truth needed for training. These sensors will not be part of the system when it will be deployed. It is also possible to compute the ground truth data using offline and more computationally intensive algorithms.

Our goal is to design a system which combines the available data and partial domain knowledge for filtering in SS models. In particular, the real-time state estimator is required to be able to learn from data to recover \mathbf{x}_t from the past observations $\{\mathbf{y}_\tau\}_{\tau=1}^t$ for SS models as in (1), where:

- Knowledge of the distribution of the noise signals \mathbf{e}_t and \mathbf{v}_t is not available.
- The functions $\mathbf{f}(\cdot)$ and $\mathbf{h}(\cdot)$ can be non-linear.
- The functions $\mathbf{f}(\cdot)$ and $\mathbf{h}(\cdot)$ may be inaccurately known.

Finally, the inference complexity of the DD state estimator should be at the same order (and preferably smaller) of that of MB filters, such as the EKF.

D. Related Work

The combination of machine learning and SS models, and more specifically the use of KF, is the focus of a growing research attention. To frame the current work in the context of the existing literature, we next provide a brief overview of relevant works in this area. We begin by presenting the main MB approaches from the classical literature, after which we discuss the current leading approaches for combining deep learning with SS models.

1) *Classical MB Approaches*: While the original KF assumes linear SS models, many problems encountered in practice are governed by non-linear dynamical equations. Non-linear variations of the KF based on an analytical linearization of the SS model were proposed shortly after the introduction of the original KF; these variants are referred to as the quasi-linear KF or the EKF [5]. A more recent extension of the KF for non-linear dynamics with Gaussian noise is the UKF [9] which is based on numerical integration; additional KF variants which rely on numerical integration are the Gauss-Hermite Quadrature [23] and the Cubature KF [24]. An alternative approach for real-time state estimation via recursive Bayesian estimation uses Monte-Carlo based filters. This approach accommodates the sequential particle filter (PF) and its variants, which are not limited to the assumption of

Gaussian noise [25], [26]. All of these MB estimators require accurate knowledge of the underlying SS model, and their performance is typically degraded in the presence of model mismatch.

2) *Deep Learning Approaches*: deep learning approaches for inference over SS models can be broadly divided into the same main categories presented in Subsection II-B. Namely, approaches that consider the task of observations generation, and approaches that consider the task of state recovery. The former usually deals with a high dimensional observations, using deep learning to encode the high dimensional observations to a latent state on which an efficient inference can be done using the KF and its variations. This is often achieved using a deep generative model, most commonly a Variational Autoencoder, combined with SS aware processing of the latent representation as in [27]–[32]. Such approaches can typically not be directly applied to state recovery, as we consider here, and the learning procedure tends to be complex and prone to approximation errors.

In the context of state estimation, one approach is use machine learning methods to directly estimate the SS model parameters, which are then substituted into the KF (or a specific variant), as done in [33]–[36]. The drawback of this strategy is that it is limited to the specific form of the SS model considered, e.g., a linear Gaussian SS model. An alternative approach is to utilize deep learning modules for extracting features which are used for inference using Kalman filtering or other form of SS model inference [37]–[41]. This form of learned filtering is typically designed for unknown or highly complex SS models, such as, e.g., those encountered in computer vision [41], while we focus on setups with partial domain knowledge, as detailed in Subsection II-C. Also related is the work [42], which applied focused on offline state estimation a graph neural network in parallel to the Kalman smoother to improve its accuracy via neural augmentation. Since the estimation was performed by an iterative message passing over the entire time horizon, it cannot be adopted with low complexity to the filtering task.

E. Model-Based Kalman Filtering

Our proposed KalmanNet detailed in the following section is based on the MB KF, which is a linear recursive estimator. In every time step t , the KF produces a new estimate \mathbf{x}_t using only the previous estimate $\hat{\mathbf{x}}_{t-1}$ as a sufficient statistic and the new observation \mathbf{y}_t . As a result, the computational complexity of the KF does not grow in time.

The direct extension of this algorithm to non-linear models is the EKF, which linearizes the SS model. The EKF can be described by a two-step procedure: *prediction* and *update*, where in each step we compute the first- and second-order statistical moments.

- 1) The first step *predicts* the statistical moments based on the previous a posteriori estimates. Specifically, the first-order moments are predicted via

$$\hat{\mathbf{x}}_{t|t-1} = \mathbf{f}(\hat{\mathbf{x}}_{t-1}), \quad (2a)$$

$$\hat{\mathbf{y}}_{t|t-1} = \mathbf{h}(\hat{\mathbf{x}}_{t|t-1}). \quad (2b)$$

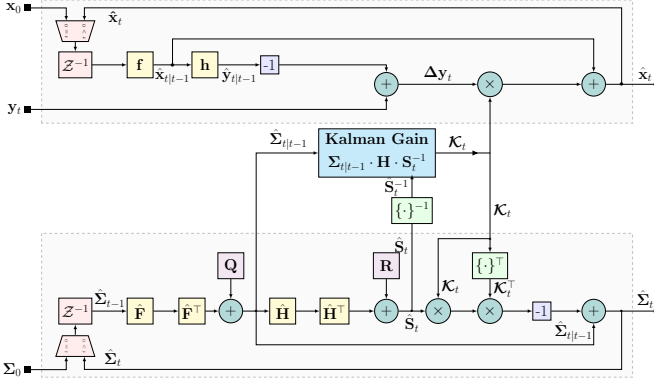


Fig. 2: EKF block diagram. Here, Z^{-1} is the unit delay.

The first-order statistical moments are propagated through the non-linearity, and the second-order statistical moments are evaluated by the first-order Taylor series expansion. When $f(\cdot)$ and $h(\cdot)$ are differentiable, they can be linearized by using their partial derivative (Jacobian) matrices, denoted $J_f(\cdot)$ and $J_h(\cdot)$, respectively, evaluated at \hat{x}_{t-1} and $\hat{x}_{t|t-1}$. Namely, by writing

$$\hat{F}_t = J_f(\hat{x}_{t-1}), \quad \hat{H}_t = J_h(\hat{x}_{t|t-1}), \quad (3)$$

the predicted second-order moments are computed as

$$\hat{\Sigma}_{t|t-1} = \hat{F}_t \cdot \hat{\Sigma}_{t-1} \cdot \hat{F}_t^\top + Q, \quad (4a)$$

$$\hat{S}_{t|t-1} = \hat{H}_t \cdot \hat{\Sigma}_{t|t-1} \cdot \hat{H}_t^\top + R. \quad (4b)$$

- 2) In the *update* step, the a posteriori moments are computed based on the a priori moments. The pivot computation for this step is the Kalman gain \mathcal{K}_t

$$\mathcal{K}_t = \hat{\Sigma}_{t|t-1} \cdot \hat{H}_t^\top \cdot \hat{S}_{t|t-1}^{-1}. \quad (5)$$

By (5), the KG depends only on the second-order statistical moments and not on the data (observations). Given the new observation y_t , the innovation process Δy_t is computed as

$$\Delta y_t = y_t - \hat{y}_{t|t-1}, \quad (6)$$

from which the state estimate (the first-order posterior) is obtained via

$$\hat{x}_t = \hat{x}_{t|t-1} + \mathcal{K}_t \cdot \Delta y_t. \quad (7)$$

The second-order posterior is then computed as

$$\hat{\Sigma}_t = \hat{\Sigma}_{t|t-1} - \mathcal{K}_t \cdot \hat{S}_{t|t-1} \cdot \mathcal{K}_t^\top. \quad (8)$$

An illustration of the EKF is depicted in Fig. 2.

When the evolution and observation functions are linear, i.e., there exist matrices F, H such that

$$f(x) = F \cdot x, \quad h(x) = H \cdot x, \quad (9)$$

then the EKF coincides with the KF. When the noise is Gaussian, and the SS model parameters are fully known, the KF is the MMSE estimator. However, when $f(\cdot)$ and/or $h(\cdot)$ are highly non-linear, the local linearity approximation may not hold, and the EKF can result in degraded performance. This motivates the augmentation of the EKF into the deep learning-aided KalmanNet, detailed in the following section.

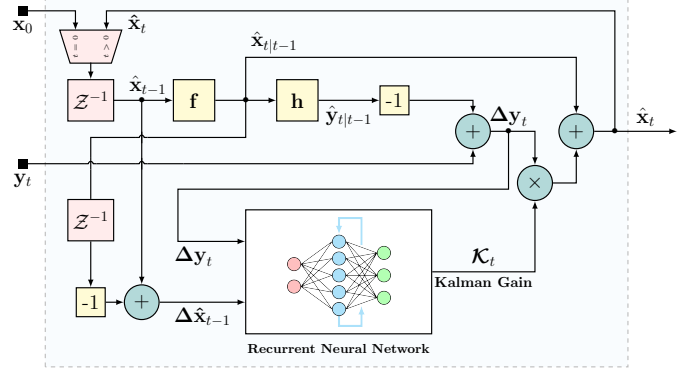


Fig. 3: KalmanNet block diagram.

III. KALMANNET

Here, we present *KalmanNet*; a hybrid, interpretable, data efficient architecture for real-time state estimation in non-linear dynamical systems with partial domain knowledge. KalmanNet combines the MB Kalman filtering with an RNN to cope with model mismatch and non-linearities. To introduce KalmanNet, we begin by explaining its high level operation in Subsection III-A. Then we present the features processed by its internal RNN and the specific architectures considered for implementing this learned model in Subsections III-B-III-C. Finally, we provide a discussion in Subsection III-E.

A. High Level Architecture

We formulate KalmanNet by identifying the specific computations of the KF that are based on unavailable knowledge. As detailed in Subsection II-C, the functions f and h are known (though perhaps inaccurately); yet the covariance matrices Q and R are unavailable. These missing statistical moments are used in MB Kalman filtering only for computing the KG (see Fig. 2). Consequently, we design KalmanNet to learn the KG from data, and combine the learned KG in the overall KF flow. This high level architecture is illustrated in Fig. 3.

In particular, similarly to the KF, in each time instance t KalmanNet estimates \hat{x}_t in two steps; *prediction* and *update*.

- The *prediction* step is the same as in the MB EKF, except that only the first-order statistical moments are predicted. In particular, KalmanNet first computes the current prior estimate $\hat{x}_{t|t-1}$ by a state-evolution forward pass, using the previous posterior estimate \hat{x}_{t-1} and the evolution function f as in (2a). Then, using the observation function h , we can compute an estimate for the current observation $\hat{y}_{t|t-1}$ via (2b).
- The *update* step uses the current observation y_t . As in the MB EKF, the innovation Δy_t is computed via (6), and the current posterior state-estimate \hat{x}_t is obtained using (7). Nonetheless, as opposed to the MB KF, here the computation of the KG is not given explicitly, but is learned from data using an RNN, as illustrated in Fig. 3. The inherent memory of RNNs allows to implicitly track the second-orders statistical moments, without requiring knowledge of the underlying noise statistics.

Designing an RNN to learn how to compute the KG as part of an overall KF flow requires answers to three key questions:

- 1) From which input features (signals) will the network learn the KG?
- 2) What should be the architecture of the internal RNN?
- 3) How will this network be trained from data?

In the following sections we address these questions.

B. Input Features

The MB KF and its variants compute the KG from knowledge of the underlying statistics. In order to implement such computations in a learned fashion, one must provide to a neural network inputs (features) that capture the knowledge needed to evaluate the KG. The dependence of \mathcal{K}_t on the statistics of the observations and the state process indicates that in order to track it, the RNN should be provided with inputs containing statistical information of the observations \mathbf{y}_t and the state-estimate $\hat{\mathbf{x}}_{t-1}$ in every time step t . Therefore, the following quantities which are related to the unknown statistical relationship of the SS model can be used as input features to the RNN:

- F1 The *observation difference* $\Delta \tilde{\mathbf{y}}_t = \mathbf{y}_t - \mathbf{y}_{t-1}$.
- F2 The *innovation difference* $\Delta \mathbf{y}_t = \mathbf{y}_t - \hat{\mathbf{y}}_{t|t-1}$.
- F3 The *forward evolution difference* $\Delta \tilde{\mathbf{x}}_t = \hat{\mathbf{x}}_{t|t} - \hat{\mathbf{x}}_{t-1|t-1}$. This quantity represents the difference between two consecutive posterior state estimates, where in time instance t , the available feature is $\Delta \tilde{\mathbf{x}}_{t-1}$.
- F4 The *forward update difference* $\Delta \hat{\mathbf{x}}_t = \hat{\mathbf{x}}_{t|t} - \hat{\mathbf{x}}_{t|t-1}$, i.e., the difference between the posterior state estimate to the prior state estimate, where again in time instance t we use $\Delta \hat{\mathbf{x}}_{t-1}$.

Features **F2** and **F4** encapsulate the uncertainty of our state estimate. The difference operation removes the predictable components, and thus the differences time series are mostly affected by the noise statistics that we wish to learn. Features **F1** and **F3** encapsulate information about the state-evolution. The RNN described in Fig. 3 can use all the features, although extensive empirical evaluation suggests that the specific choice of combination of features depends on the problem at hand. Our empirical observations indicate that good combinations are $\{\mathbf{F1}, \mathbf{F2}, \mathbf{F4}\}$ and $\{\mathbf{F1}, \mathbf{F3}, \mathbf{F4}\}$.

C. Neural Network Architecture

The internal neural network used by KalmanNet uses the features discussed in the previous section to compute the KG. It follows from (2) and (5) that computing the KG \mathcal{K}_t involves tracking the second-order statistical moment Σ_t . The recursive nature of the KG computation indicates that its learned module should involve an internal memory element as an RNN to track it.

We consider two architectures for the KG computing RNN. The first aims at using the internal memory of RNNs to jointly track the underlying second-order statistical moments required for computing the KG in an implicit manner. To that aim, we use GRU cells [14] whose hidden state is of the size of some integer product of $m^2 + n^2$, which is the joint dimensionality of the tracked moments $\hat{\Sigma}_{t|t-1}$ and $\hat{\mathbf{S}}_t$ in (4). In particular, we first use a fully connected (FC) input layer whose output,

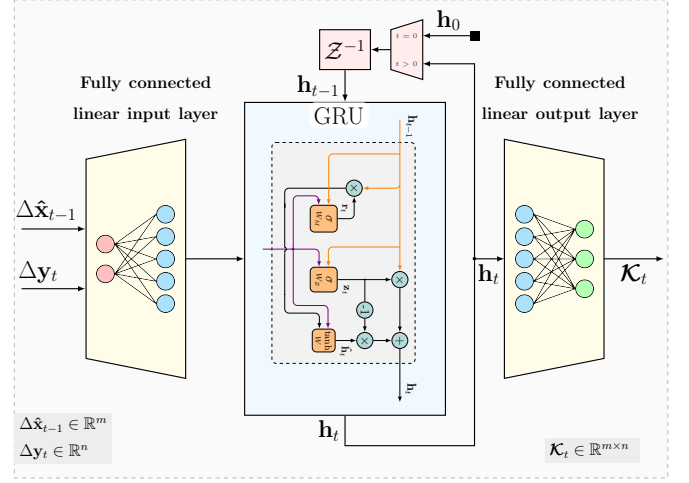


Fig. 4: KalmanNet RNN block diagram (architecture #1). In this illustration, the input features are **F2** and **F4**.

denoted ψ_t , is the input to the GRU. The GRU state vector \mathbf{h}_t is mapped into the estimated KG $\mathcal{K}_t \in \mathbb{R}^{m \times n}$ using an output FC layer with $m \cdot n$ neurons. The resulting architecture is illustrated in Fig. 4. While the illustration in Fig. 4 uses a single GRU layer, one can also utilize multiple layers to increase the capacity and abstractness of the network, as we do in the numerical study reported in Subsection IV-E.

The first architecture illustrated in Fig. 4 does not directly design the hidden state of the GRU to correspond to the unknown second-order statistical moments which are tracked by the MB EKF. As such, it uses a relatively large number of state variables which are expected to provide the required tracking capacity, e.g., in the numerical study in Section IV we set the dimensionality of \mathbf{h}_t to be $10 \cdot (m^2 + n^2)$. This often results in substantial over-parametrization, as the number of GRU parameters grows quadratically with the number of state variables [43]. Therefore, we also propose an alternative architecture which uses separate GRU cells for each tracked second-order moment. The resulting architecture illustrated in Fig. 5 is composed of three GRU layers, connected in a cascade with dedicated input and output FC layers. The first GRU layer tracks the unknown state noise covariance \mathbf{Q} , thus tracking m^2 variables. Similarly, the second and third GRUs track the predicted moments $\hat{\Sigma}_{t|t-1}$ and $\hat{\mathbf{S}}_t$, thus having m^2 and n^2 hidden state variables, respectively. The interconnection between those GRUs, where the learned \mathbf{Q} is used to compute $\hat{\Sigma}_{t|t-1}$, which in turn is used to obtain $\hat{\mathbf{S}}_t$, while both $\hat{\Sigma}_{t|t-1}$ and $\hat{\mathbf{S}}_t$ are involved in producing \mathcal{K}_t , corresponds to the second moments equations (4), (5), and (8).

The second architecture is more directly tailored towards the formulation of the SS model and the operation of the EKF compared to the simpler first architecture. As such, the second architecture provides lesser abstraction, i.e., it is expected to be more constrained in the family of mappings it can learn compared the first architecture, while as a result also requiring less trainable parameters. For instance, in the numerical study reported in Subsection IV-D, utilizing the first architecture requires the order of $5 \cdot 10^5$ trainable parameters, while the second architecture utilizes merely $2.5 \cdot 10^4$ parameters. As

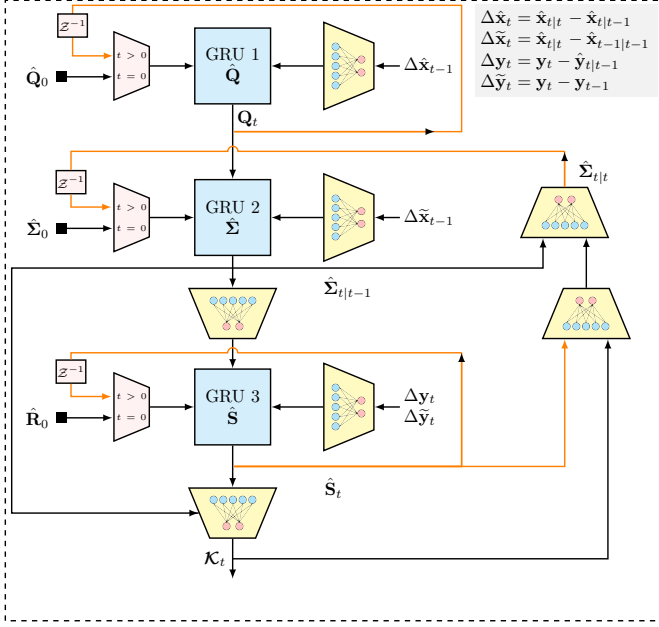


Fig. 5: KalmanNet RNN block diagram (architecture #2).

our numerical evaluations show that these two architecture often achieve similar mean-squared error (MSE) performance of KalmanNet, in the majority of the numerical study we use the simpler first architecture, while the second architecture is utilized in the experimental study considering the tracking of Lorenz attractor detailed in Subsection IV-D.

D. Training Algorithm

KalmanNet is trained using the available labeled data set in a supervised fashion. Since the state variable \mathbf{x}_t takes values in a continuous set \mathbb{R}^m , we use the MSE loss, which for estimating \mathbf{x}_t using $\hat{\mathbf{x}}_{t|t}$ is given by $\mathcal{L} = \|\mathbf{x}_t - \hat{\mathbf{x}}_{t|t}\|^2$. While we use a neural network for computing the KG rather than for directly producing the estimate $\hat{\mathbf{x}}_{t|t}$, we train KalmanNet end-to-end. By doing so, we build upon the ability to backpropagate the MSE loss to the computation of the KG. The ability to obtain the loss gradient with respect to the KG from the output of KalmanNet follows from the fact that

$$\begin{aligned} \frac{\partial \mathcal{L}}{\partial \mathcal{K}_t} &= \frac{\partial \|\mathcal{K}_t \Delta \mathbf{y}_t - \Delta \mathbf{x}_t\|^2}{\partial \mathcal{K}_t} \\ &= 2 \cdot (\mathcal{K}_t \cdot \Delta \mathbf{y}_t - \Delta \mathbf{x}_t) \cdot \Delta \mathbf{y}_t^\top, \end{aligned} \quad (10)$$

where $\Delta \mathbf{x}_t \triangleq \mathbf{x}_t - \hat{\mathbf{x}}_{t|t-1}$. The gradient computation in (10) indicates that one can learn the computation of the KG by training KalmanNet end-to-end using the MSE loss.

The data set used for training is comprised of N trajectories which can be of varying lengths. Namely, by letting T_i be the length of the i th training trajectory, the data set is given by $\mathcal{D} = \{(\mathbf{Y}_i, \mathbf{X}_i)\}_{i=1}^N$, where

$$\mathbf{Y}_i = [\mathbf{y}_1^{(i)}, \dots, \mathbf{y}_{T_i}^{(i)}], \quad \mathbf{X}_i = [\mathbf{x}_0^{(i)}, \mathbf{x}_1^{(i)}, \dots, \mathbf{x}_{T_i}^{(i)}]. \quad (11)$$

Specifically, we use the ℓ_2 regularized MSE loss. By letting Θ be the trainable parameters of the RNN, this loss measure

is given by

$$\ell_i(\Theta) = \frac{1}{T_i} \sum_{t=1}^{T_i} \left\| \hat{\mathbf{x}}_t(\mathbf{y}_t^{(i)}; \Theta) - \mathbf{x}_t^{(i)} \right\|^2 + \gamma \cdot \|\Theta\|^2, \quad (12)$$

where γ is a regularization coefficient. To optimize Θ , we use a variant of mini-batch stochastic gradient descent in which for every batch indexed by k , we choose $M < N$ trajectories indexed by i_1^k, \dots, i_M^k , computing the mini-batch loss as

$$\mathcal{L}_k(\Theta) = \frac{1}{M} \sum_{j=1}^M \ell_{i_j^k}(\Theta). \quad (13)$$

Since KalmanNet is a recursive architecture with both an external recurrence and an internal RNN, we use the Backpropagation through time (BPTT) algorithm [44] to train it. Specifically, we unfold KalmanNet across time with shared network parameters, and then compute a forward- and backward gradient estimation pass through the network. We consider three different variations of applying the BPTT algorithm for training KalmanNet:

- V1 Direct application of BPTT, where for each training iteration the gradients are computed over the entire trajectory.
- V2 An application of the truncated BPTT algorithm [45]. Here, given a data set of long trajectories (e.g., $T = 3000$ time steps), each long trajectory is divided into multiple short trajectories (e.g., $T = 100$ time steps), which are shuffled and used during training.
- V3 An alternative application of truncated BPTT, where we truncate each trajectory to a fixed (and relatively short) length, and train using these short trajectories.

Overall, directly applying BPTT via V1 is computationally expensive, and may be unstable. Therefore, a favourable approach is to use truncated BPTT as in V2 as a warm-up phase (train first on short trajectories) in order to stabilize its learning process, after which KalmanNet is tuned using V1. The procedure in V3 is most suitable for systems that are known to be likely to quickly converge to a steady-state (e.g., linear SS models). In our numerical study reported in Section IV we utilize all three approaches.

E. Discussion

KalmanNet is designed to operate in a hybrid DD/MB manner, integrating deep learning into the classical EKF procedure. This operation, which is based on identifying the specific noise-model-dependent computations of the KF and replacing them with a dedicated RNN integrated in the EKF flow, benefits from the individual strengths of both DD and MB approaches. Compared with MB Kalman filtering, KalmanNet is more robust to model mismatch, as demonstrated in Section IV. In particular, MB Kalman filtering is sensitive to inaccuracies in the underlying SS model, e.g., in $\mathbf{f}(\cdot)$ and $\mathbf{h}(\cdot)$, while KalmanNet can overcome such uncertainty by learning an alternative KG that yields accurate estimation. Furthermore, KalmanNet is derived for SS models when noise statistics are not specified explicitly. The direct strategy to implement the EKF in such setups is to use the data to estimate \mathbf{Q} and \mathbf{R} , either directly from the data or by backpropagating

through the operation of the EKF as in [36], and utilize these estimates to compute the KG. As covariance estimation can be a challenging task when dealing with high-dimensional signals, KalmanNet bypasses this need by directly learning the KG. Finally, the computation complexity for each time step t is also linear in the RNN dimensions and does not involve matrix inversion. This implies that KalmanNet is a good candidate to apply for high dimensional SS model and on computationally limited devices.

Compared with purely DD state estimation, KalmanNet benefits from its model-awareness and the fact that its operation follows the flow of the MB EKF rather than being utilized as a black-box. As numerically observed in Section IV, KalmanNet achieves improved MSE compared with utilizing RNNs for end-to-end state estimation, as well as approach the MMSE performance achieved by the MB KF in linear Gaussian SS models. Furthermore, the fact that KalmanNet preserves the flow of the EKF implies that the intermediate features exchanged between its modules have a specific operation meaning, providing interpretability which is often scarce in end-to-end deep learning systems. Finally, the fact that KalmanNet learns to compute the KG indicates the possibility of providing not only estimates of the state \mathbf{x}_t , but also a measure of confidence in this estimate, as the KG can be related to the covariance of the estimate. Nonetheless, we leave the detailed study of this characteristic of the MB operation of KalmanNet for future investigation.

These combined gains of KalmanNet over purely MB and DD approaches was recently observed in the conference paper [46], which utilized an early version of KalmanNet for real-time velocity estimation in an autonomous racing car. In such setup, a variant of the MB EKF was traditionally used, and suffered from performance degradation due to inherent mismatches in the formulation of the SS model describing the problem. Nonetheless, previously proposed DD techniques relying on RNNs for end-to-end state estimation were not operable in the desired frequencies on the hardware limited vehicle control unit. It was shown in [46] that the application of KalmanNet allowed to achieve improved real-time velocity tracking compared to MB techniques while being deployed on the control unit of the vehicle.

Our design of KalmanNet gives rise to many interesting future extensions. Since we focus here on SS models where the mappings $\mathbf{f}(\cdot)$ and $\mathbf{h}(\cdot)$ are known up to some approximation errors, a natural extension of KalmanNet is to utilize dedicated neural networks to learn these mappings. Doing so is expected to allow KalmanNet to be utilized in scenarios with analytically intractable SS models, as often arises when tracking based on visual observations [41]. Additionally, while we train KalmanNet in a supervised manner using labeled data, the fact that it preserves the operation of the MB EKF which produces a prediction of the next observation $\hat{\mathbf{y}}_{t|t-1}$ on each time instance indicates the possibility of using this intermediate feature for unsupervised training. One can thus envision KalmanNet being trained offline in a supervised manner, while tracking variations in the underlying SS model in run-time by re-training in an unsupervised manner following a similar rationale to that used in [17], [18] for deep symbol detection in

time-varying communication channels. Nonetheless, we leave these exciting extensions of KalmanNet for future work.

IV. EXPERIMENTS AND RESULTS

In this section we present an extensive numerical study of KalmanNet. We consider the following numerical evaluations:

- (a) *Neural Model Selection*: In our first experimental study we evaluate the design of KalmanNet and confirm our architectural choices by comparing KalmanNet with using RNNs for end-to-end state estimation.
- (b) *Synthetic Linear Model*: Next, we consider linear SS models in which the MB KF is known to minimize the MSE. Here, we show that KalmanNet coincides with the KF, and outperforms it in the presence of model mismatch,
- (c) *Synthetic Non-Linear Model*: Our third study considers non-linear synthetic SS models, where the MB EKF is the common MB benchmark. In this study we demonstrate that KalmanNet can learn to achieve improved MSE compared to the EKF operating with full domain knowledge, due to the sub-optimality of the latter.
- (d) *Lorenz attractor*: Here, we evaluate KalmanNet for real-time tracking of the Lorenz attractor, which is a highly non-linear system with chaotic behavior. In the Lorenz attractor setup, we show how the gains of KalmanNet viewed for the synthetic problems are translated into concrete benefits for tracking a challenging chaotic system in real-time, while providing the ability to overcome crude sampling based decimation.
- (e) *Real World Dynamics*: Our last study considers localization in real world dynamics based on the Michigan NCLT data set [21], where we demonstrate the ability of KalmanNet to achieve improved capability of real-time tracking with real-life data.

Throughout the numerical study¹, and unless stated otherwise, in the experiments involving synthetic data, the SS model is generated using diagonal noise covariance matrices; i.e.,

$$\mathbf{Q} = \mathbf{q}^2 \cdot \mathbf{I}, \quad \mathbf{R} = \mathbf{r}^2 \cdot \mathbf{I}, \quad \nu \triangleq \frac{\mathbf{q}^2}{\mathbf{r}^2}. \quad (14)$$

In the following experiments the term *full information* refers to the case where KalmanNet and the MB KF (or EKF) operate with accurate SS model knowledge. Namely, the plug-in design parameters, e.g., $\mathbf{f}(\cdot)$ and $\mathbf{h}(\cdot)$, are those of the true generative model. The term *partial information* refers to the case where KalmanNet and MB Kalman filtering operate with model uncertainty, i.e., the model parameters are not equal to the SS parameters from which the data was generated. In both cases, KalmanNet does not have access to noise covariance.

In Section III we present several architectures and training mechanisms which can be used when implementing KalmanNet. In our experimental study we consider three different configurations of KalmanNet:

¹The source code used in our numerical study along with the complete set of hyper-parameters used in each numerical evaluation can be found online at https://github.com/KalmanNet/KalmanNet_TSP.

- C1 KalmanNet architecture #1 with input features $\{F2, F4\}$, and with training algorithm V3
- C2 KalmanNet architecture #1 with input features $\{F2, F4\}$, and with training algorithm V1
- C3 KalmanNet architecture #1 with input features $\{F1, F3, F4\}$, and with training algorithm V2.
- C4 KalmanNet architecture #2 with all input features, and with training algorithm V1.

In all our experiments KalmanNet was trained using the Adam optimizer [47].

A. Neural Model Selection

In this study we evaluate the design of KalmanNet and confirm our architectural choices. We generate a synthetic data set using a 2×2 linear SS model where the matrices F and H in (9) take the controllable canonical and inverse canonical forms, respectively, and $\nu = 0$ [dB]. For this setup, we compare KalmanNet with setting C1 to two RNN based architectures of similar capacity applied for end-to-end state estimation:

- *Vanilla RNN* directly maps the observed y_t to an estimate of the state \hat{x}_t .
- *MB RNN* imitates the Kalman filtering operation by first recovering $\hat{x}_{t|t-1}$ using domain knowledge, i.e., via (2a), and then uses the RNN to estimate an increment $\Delta\hat{x}_t$ from the prior to posterior.

All RNNs utilize the same architecture as in KalmanNet with a single GRU layer and the same learning hyperparameters.

The learning curves are depicted in Fig. 6, where we observe how each of the key design considerations of KalmanNet affect the learning curve: the incorporation of the known SS model allows the MB RNN to outperform the vanilla RNN, although both converge slowly and fail to achieve the MMSE; using the difference sequences as input notably improves the convergence rate of the MB RNN, indicating the benefits of using the difference features as discussed in Subsection III-B; and learning is further improved by using the RNN for recovering the KG as part of the KF flow, as done by KalmanNet, rather than for directly estimating x_t .

In this experiment whose results are reported in Fig. 6 we test the pre-trained models on trajectories with the same length that it was trained on, namely $T = 20$. To further evaluate the gains of the hybrid architecture of KalmanNet, we check if its learning is transferable. Namely, we test the pretrained models using trajectories with different initial conditions and a longer time horizon ($T = 200$) than the one on which it was trained. The results, summarized in Table I, show that KalmanNet maintains achieving the MMSE, implying that it learned to carry out Kalman filtering. The MB RNN and vanilla RNN are more than 50 [dB] from the MMSE, implying that their learning is not transferable and that they do not learn to implement Kalman filtering. However, when provided with the difference features as we proposed in Subsection III-B, the DD systems are shown to be applicable in longer trajectories, with KalmanNet achieving MSE within a minor gap of that achieved by the MB KF. The results of this study validate the considerations used in designing KalmanNet for the DD filtering problem discussed in Subsection II-C.

TABLE I: Test MSE in [dB] when trained using $T = 20$.

Test T	Vanilla RNN	MB RNN	MB RNN, diff.	KalmanNet	KF
20	-20.98	-21.53	-21.92	-21.92	-21.97
200	58.14	36.8	-21.88	-21.90	-21.91

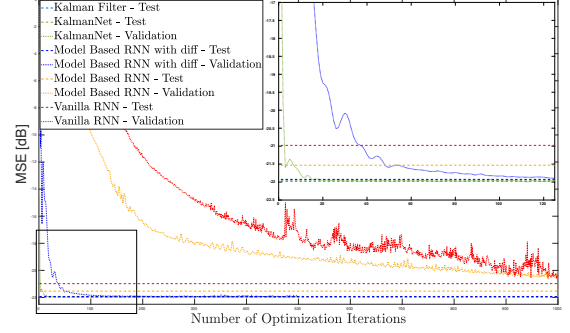


Fig. 6: Learning curves for DD state estimation.

B. Synthetic Linear Model

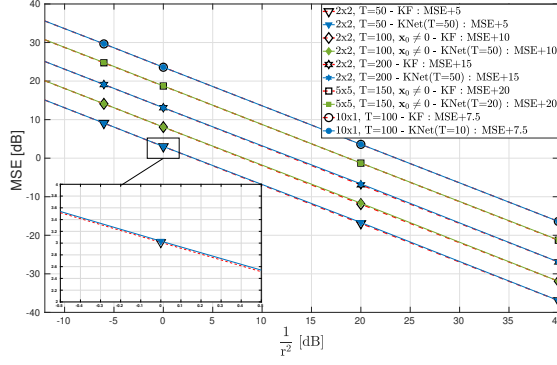
Our second experimental study compares KalmanNet to the MB KF for different forms of linear system dynamics. We evaluate both algorithms on a synthetic data set, where we again set F and H to take the controllable canonical and inverse canonical forms, respectively, and $\nu = 0$ [dB]. As opposed to the neural model selection setup, here we use models with different dimensions, set to 2×2 , 5×5 , and 10×1 . In this experiment we test and train KalmanNet with trajectories of the same length using setting C2.

The first experiment compares the MSE achieved by KalmanNet to that of the KF with full information, which represents the MMSE. The MSE comparison versus the inverse observations noise level $\frac{1}{r^2}$ for different trajectory lengths $T \in \{50, 100, 150, 200\}$ is depicted in Fig. 7a. We clearly observe in Fig. 7a KalmanNet indeed learns to implement Kalman filtering and achieve the MMSE in all considered setups. The results demonstrate again that KalmanNet is not tailored to the trajectories presented during training, and it learns to do training with dependency only on the SS model.

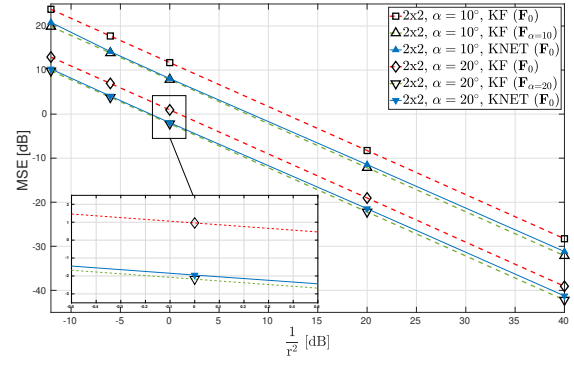
Next, we study the robustness of KalmanNet to model uncertainty, i.e., when it operates with partial information. Here, we focus on a 2×2 SS model, with $T = 20$, and $\nu = 0$ [dB]. Model uncertainty is achieved by plugging in F_0 as a design evolution matrix for both KalmanNet and the MB KF, while the data is generated from an SS model based on a rotated evolution matrix F_{α° .

$$F_{\alpha^\circ} = \begin{pmatrix} \cos \alpha & -\sin \alpha \\ \sin \alpha & \cos \alpha \end{pmatrix} \cdot F_0, \quad \alpha \in \{10^\circ, 20^\circ\}. \quad (15)$$

Such scenarios represent a setup in which the analytical approximation of the SS model used as a plugged-in parameter in the KF flow differs from the true model. The resulting achieved MSE versus $\frac{1}{r^2}$ depicted in Fig. 7b demonstrate that KalmanNet achieves a 3 [dB] gain over KF. In particular, despite the fact that KalmanNet implements the KF with inaccurate F , it learns to apply an alternative KG, resulting in MSE within a minor gap from the MMSE; i.e., from the KF with the true F_{α° plugged in.



(a) Full information: KalmanNet converges to MMSE.



(b) Partial information: KalmanNet outperforms KF by 3 [dB].

Fig. 7: Linear SS model - an MSE offset was added as specified in the legend for each curve to avoid overlapping.

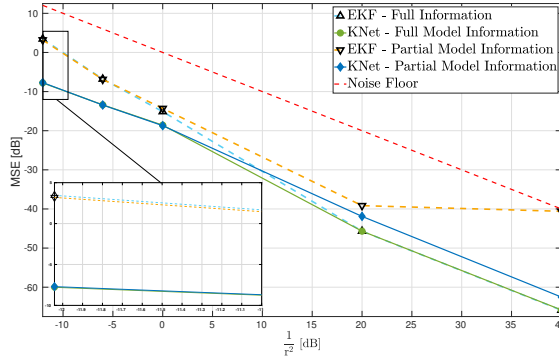


Fig. 8: Non-linear SS model. KalmanNet outperforms EKF.

C. Synthetic Non-Linear Model

Next, we consider a non-linear SS model. Here, the state evolution and observation functions are computed in a component-wise manner via

$$\mathbf{f}(\mathbf{x}) = \alpha \cdot \sin(\beta \cdot \mathbf{x} + \phi) + \delta, \quad \mathbf{x} \in \mathbb{R}^2, \quad (16a)$$

$$\mathbf{h}(\mathbf{x}) = a \cdot (b \cdot \mathbf{x} + c)^2, \quad \mathbf{y} \in \mathbb{R}^2. \quad (16b)$$

The parameters of (16) used in our numerical study are summarized in Table II. We set $T = 100$ and $\nu = 0$ [dB], and again use KalmanNet with setting C2.

The MSE values for different levels of observations noise r^2 achieved by KalmanNet compared with the MB EKF are depicted in Fig. 8 for both full as well as partial model information. We observe in Fig. 8 that for full information and in the low noise regime, EKF achieves the lowest MSE values, due to its ability to approach the MMSE in such setups. It is also noted that KalmanNet achieves the same performance. For higher noise levels, i.e., for $\frac{1}{r^2} \leq 0$ [dB], the MB EKF fails to overcome the non-linearity, and a significant MSE degradation is observed. Nonetheless, by learning to compute the KG from data, KalmanNet manages to overcome this pitfall and achieves superior MSE.

In the presence of partial model information, the state evolution parameters used by the filters slightly differ from the true model, resulting a notable degradation in the EKF performance due to the model mismatch. In all experiments,

TABLE II: Non-linear toy problem parameters.

	α	β	ϕ	δ	a	b	c
Full	0.9	1.1	0.1π	0.01	1	1	0
Partial	1	1	0	0	1	1	0

KalmanNet overcomes such mismatches, and its performance is within a minor gap of that achieved when using full information for such setups. We thus conclude that in the presence of harsh non-linearities as well as model uncertainty due to inaccurate approximation of the underlying dynamics, where MB variations of the KF fail, KalmanNet learns to approach the MMSE while maintaining the real-time operation and low complexity of the KF.

D. Lorenz Attractor

The Lorenz attractor is a three-dimensional chaotic solution to the Lorenz system of ordinary differential equations. This synthetically generated system is chosen because it demonstrates the task of online tracking a highly non-linear trajectory, and it also demonstrates a real world practical challenge of handling mismatches due to sampling a continuous-time process into discrete-time. In particular, we consider a continuous-time state process denoted \mathbf{x}_τ with $\tau \in \mathbb{R}^+$. The noiseless state evolution of the Lorenz attractor is given by the continuous-time differential equation:

$$\frac{\partial}{\partial \tau} \mathbf{x}_\tau = \mathbf{A}(\mathbf{x}_\tau) \cdot \mathbf{x}_\tau, \quad \mathbf{A}(\mathbf{x}) = \begin{pmatrix} -10 & 10 & 0 \\ 28 & -1 & -x_1 \\ 0 & x_1 & -\frac{8}{3} \end{pmatrix}. \quad (17)$$

We sample the continuous-time differential system (17) with sampling interval $\Delta\tau$ to obtain a discrete-time state process \mathbf{x}_t corresponding to time instance $\tau = t \cdot \Delta\tau$, with $t \in \mathbb{Z}^+$. The state evolution is approximated by taking a Taylor series of order J of (17), resulting in the (noiseless) state evolution model

$$\mathbf{x}_{t+1} = \mathbf{F}(\mathbf{x}_t) \cdot \mathbf{x}_t, \quad (18)$$

with

$$\mathbf{F}(\mathbf{x}) = \exp(\mathbf{A}(\mathbf{x}) \cdot \Delta\tau) \approx \mathbf{I} + \sum_{j=1}^J \frac{(\mathbf{A}(\mathbf{x}) \cdot \Delta\tau)^j}{j!}. \quad (19)$$

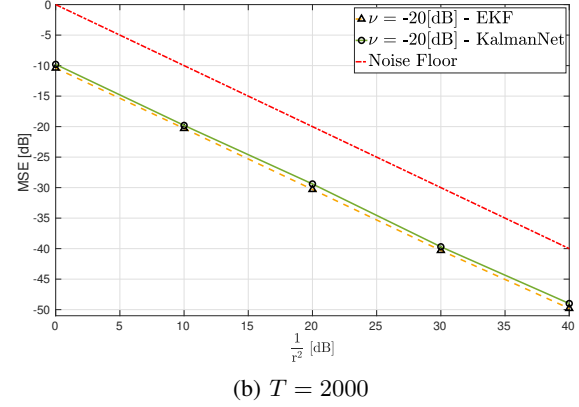
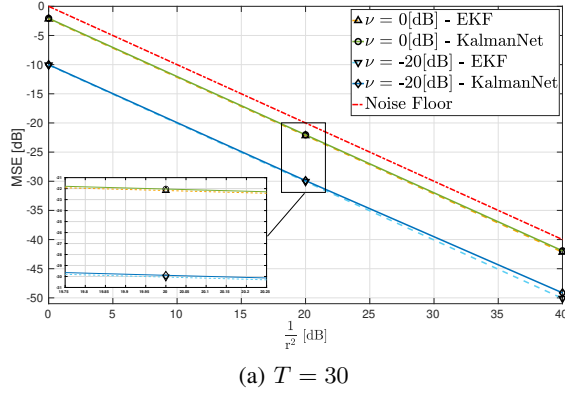


Fig. 9: Lorenz attractor, full information, identity \mathbf{h} .

This mismatch induced by the approximation in (19) becomes negligible as J grows. We thus generate data from a noisy version of the Lorenz attractor SS model (18) while computing the Taylor series expansion in (19) with order $J = 5$. Unless stated otherwise, we use sampling interval of $\Delta\tau = 0.02$.

Noisy state observations - Full information: We start by comparing KalmanNet to EKF when both filters use the state evolution matrix \mathbf{F} computed via (19) with $J = 5$. Further, we set \mathbf{h} to be the identity transformation, such that the observations are noisy versions of the true state. In Fig. 9a we depict the MSE achieved by the filters versus $\frac{1}{r^2}$ for both $\nu = 0$ [dB] as well as $\nu = -20$ [dB], when the trajectory length is $T = 30$, and KalmanNet is implemented with configuration C2. We observe in such scenarios, where there is no model mismatch, that the EKF and KalmanNet achieve the roughly the same MSE, while the latter does not require knowledge of the noise statistics.

Next, we increase the trajectory length to $T = 2000$, while training KalmanNet on short trajectories of length $T = 30$ using setting C3. Despite being trained on short trajectories, KalmanNet is empirically shown to achieve excellent MSE performance, as observed in Fig 9b. For comparison, applying the EKF with full model information achieves unstable state tracking performance, with MSE values surpassing 30 [dB]. To stabilize the EKF, we had to perform a grid search using the available data set for optimizing the process noise \mathbf{Q} used by the filter. The MSE results depicted in Fig. 9b are those achieved by the EKF after this optimization.

Noisy state observations - Partial information: We proceed to evaluate KalmanNet under partial model information. We consider two possible sources of model mismatch arising in the Lorenz attractor setup: State evolution mismatch due to use of a Taylor series approximation of insufficient order and observation model mismatch as a result of misalignment. In both studies we use relatively long trajectories of length $T = 2000$ and fix $\nu = -20$ [dB]. Following the observations in Fig. 9b, we use the training data to optimize the matrix \mathbf{Q} used by the MB EKF via grid search, setting it to the one using the which EKF achieves the minimal MSE. This optimization is necessary for the EKF to consistently converge, as also observed in the study reported in Fig. 9b.

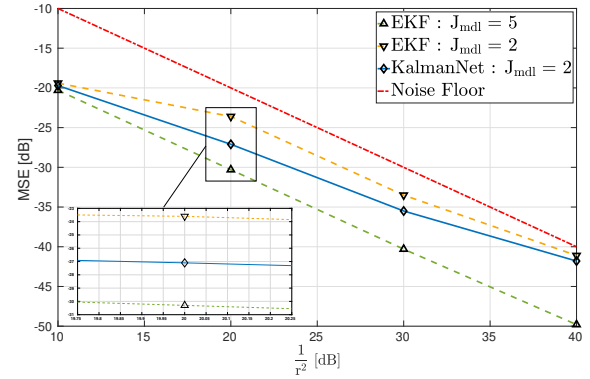


Fig. 10: Lorenz attractor, partial information with state-evolution mismatch, identity \mathbf{h} , $T = 2000$.

For state evolution mismatch, both KalmanNet and the MB EKF operate with a crude approximation of the evolution dynamics obtained by computing (19) with $J_{\text{mdl}} = 2$ while the data is generated with an order $J = 5$ Taylor series expansion. We again set \mathbf{h} to be the identity mapping. The results, depicted in Fig. 10, demonstrates that KalmanNet (with setting C4) learns to partially overcome this model mismatch outperforming the MB EKF operating with the same level of partial information.

The presence of mismatch in the observations model is simulated by introducing misalignment. In particular, instead of applying KalmanNet and the MB EKF with the plug in parameter \mathbf{h} set to the identity mapping, it is set to the identity matrix rotated by merely 1° , due to, e.g., misaligned sensors. The resulting MSE values versus $\frac{1}{r^2}$ are depicted in Fig. 11, where KalmanNet uses setting C3. Our experimental results demonstrate the ability of KalmanNet to learn from data to overcome such mismatches and to notably outperform the MB EKF, which is sensitive to model uncertainty.

Full information, non-linear observations: Next, we consider the case where the observations are given by a non-linear function of the state, setting \mathbf{h} to represent transformation to spherical coordinates. Here, we compare KalmanNet with setting C4 to two MB state estimators designed for non-linear settings: the EKF and the PF, where the latter is implemented with 100 particles. The resulting MSE values

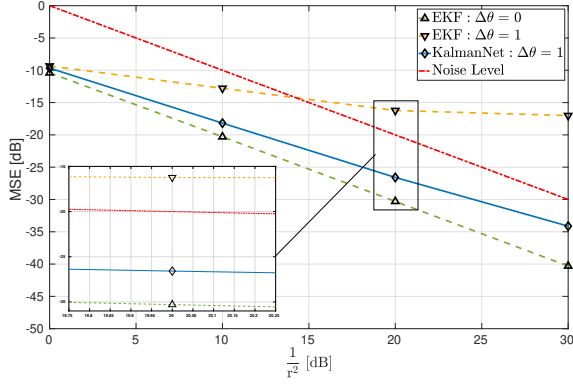


Fig. 11: Lorenz attractor, partial information with observation mismatch - $\Delta\theta = 1^\circ$, $T = 2000$.

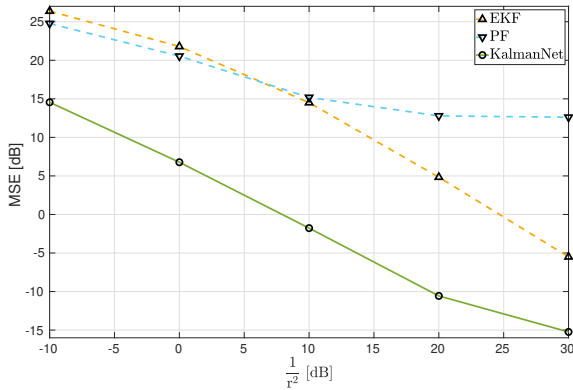


Fig. 12: Lorenz attractor, full information, non-linear \mathbf{h} .

for $T = 20$ and $\nu = 0$ [dB] are depicted in Fig. 12. We observe that in such non-linear setups, the sub-optimal MB approaches operating with full information of the SS model are substantially outperformed by KalmanNet.

Noisy state observations - Sampling mismatch: We conclude our experimental study of the Lorenz attractor setup with an evaluation of KalmanNet in the presence of sampling mismatch. Here, we generate data from the Lorenz attractor SS model with an approximately continuous-time evolution process using a dense sampling rate, set to $\Delta\tau = 10^{-5}$. We then sub-sample the noiseless observations from the evolution process by a ratio of $\frac{1}{2000}$ and get a decimated process with $\Delta\tau_d = 0.02$. This procedure results in an inherent mismatch in the SS model due to representing an (approximately) continuous-time process using a discrete-time sequence. In this experiment, no process noise was applied, the observations are again obtained with \mathbf{h} set to identity, and $\frac{1}{r^2} = 0$ [dB].

The resulting MSE values of KalmanNet with configuration **C4** compared with the EKF and the PF are reported in Table III. The results demonstrate that KalmanNet overcomes the mismatch induced by representing a continuous-time SS model in discrete-time, achieving a substantial processing gain over the MB alternatives due its learning capabilities. In Fig. 13 we visualize how this gain is translated into clearly improved tracking of the trajectory. To show that these gains of KalmanNet do not come at the cost of computationally slow inference, we detail the average inference time KalmanNet

TABLE III: MSE [dB], Lorenz attractor, sampling mismatch.

T	EKF	PF	KalmanNet
3000	-6.4322	-5.3365	-11.284

TABLE IV: Average inference time [msec], Lorenz attractor.

T	EKF	PF	KalmanNet C3	KalmanNet C4
100	290	2903	187	149

with both architecture #1 (via setting **C3**) and architecture #2 (via setting **C4**) to the MB filters when applied to a trajectory of length $T = 100$. The timings of all filters were measured on the same computer – a laptop with Intel(R) Core(TM) i7-7600U CPU @ 2.80GHz, 16GiB RAM, HD Graphics 620. We clearly observe in Table IV that KalmanNet infers faster than the classical methods, thanks to the highly efficient neural network computations and the lack of matrix inversions. Among the different architectures of KalmanNet, architecture #2 is noted to be slightly faster than architecture #1 as it uses less parameters.

E. Real World Dynamics: Michigan NCLT Data Set

In our final experiment we evaluate KalmanNet on the Michigan NCLT data set [21]. This data set is comprised of different labeled trajectories, each one contains noisy sensor readings (e.g., GPS and odometer) and the ground truth location of a moving Segway robot. Given these noisy readings, the goal of the tracking algorithm is to localize the Segway from the raw measurements at any given time.

The state vector is given by $\mathbf{x} = (p, v)^\top$, where p and v are the position and velocity respectively. We model the Segway kinematics in continuous-time on each axis using the 1-dimensional *Wiener* velocity model [48]:

$$\frac{\partial}{\partial\tau}\mathbf{x}_\tau = \begin{pmatrix} 0 & 1 \\ 0 & 0 \end{pmatrix} \cdot \mathbf{x}_\tau + \begin{pmatrix} 0 \\ 1 \end{pmatrix} \cdot w_\tau. \quad (20)$$

Here, the acceleration is modeled as a white Gaussian noise process w_t . The discrete-time state evolution with sampling

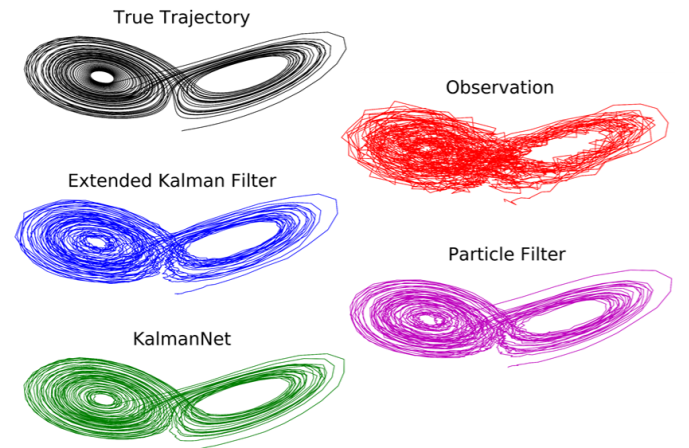


Fig. 13: Lorenz attractor with sampling mismatch, $T = 3000$.

TABLE V: Numerical MSE in [dB] for the NCLT experiment.

Baseline	EKF	KalmanNet	Vanilla RNN
25.47	25.385	22.2	40.21

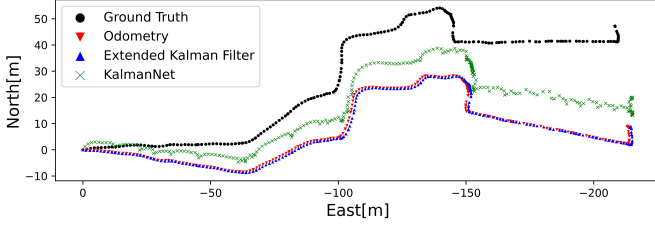


Fig. 14: NCLT data set: ground truth vs. integrated velocity, trajectory from session with date 2012-01-22 sampled at 1 Hz. interval $\Delta\tau$ is approximated as a linear SS model in which the evolution matrix \mathbf{F} and noise covariance \mathbf{Q} are given by

$$\mathbf{F} = \begin{pmatrix} 1 & \Delta\tau \\ 0 & 1 \end{pmatrix}, \quad \mathbf{Q} = \begin{pmatrix} \frac{1}{3} \cdot (\Delta\tau)^3 & \frac{1}{2} \cdot (\Delta\tau)^2 \\ \frac{1}{2} \cdot (\Delta\tau)^2 & \Delta\tau \end{pmatrix}. \quad (21)$$

The 2-dimensional evolution is then given by the block-diagonal matrices

$$\mathbf{F}_2 = \begin{pmatrix} \mathbf{F} & 0 \\ 0 & \mathbf{F} \end{pmatrix}, \quad \mathbf{Q}_2 = \begin{pmatrix} \mathbf{Q} & 0 \\ 0 & \mathbf{Q} \end{pmatrix}. \quad (22)$$

We aim at tracking the underlying state vector in both axis using solely odometry data, i.e., the observations are given by noisy velocity readings. In this case the observations obey a noisy linear model, with the following observations matrix

$$\mathbf{H}_0 = \begin{pmatrix} 0 & 1 & 0 & 0 \\ 0 & 0 & 0 & 1 \end{pmatrix}. \quad (23)$$

Due to not having a direct measurement for positioning, the odometry-based position starts drifting away. This scenario is typical for many applications where the GPS position is not available indoors and one relies on noisy odometer readings for self-localization. Inevitably, the estimate drifts from the true position. For this experiment, we arbitrarily use the session with date 2012-01-22 that consists of a single trajectory of 0.1[Km]. Sampling at 1[Hz] results in 5,850 time steps. We removed unstable readings and were left with 5,556 time steps. The trajectory was split into three sections: 85% for training (23 sequences of length $T = 200$), 10% for validation (2 sequences, $T = 200$), and 5% for testing (1 sequence, $T = 277$). We compare KalmanNet with setting **C1** to end-to-end vanilla RNN and the MB EKF, where for the latter the matrices \mathbf{Q} and \mathbf{R} are optimized through a grid search.

Fig. 14 and Table V demonstrate the superiority of KalmanNet for such scenarios. EKF blindly follows the odometer trajectory and is incapable of accounting for the drift, producing a very similar or even worse estimation than the integrated velocity. The vanilla RNN, which is agnostic of the motion model, fails to localize. KalmanNet overcomes the errors induced by the noisy odometer observations, and provides the most accurate real-time locations, demonstrating the gains of combining MB KF-based inference with integrated DD modules for real world applications.

V. CONCLUSIONS

In this work we presented KalmanNet, which combines deep learning with the classic KF. Our design identifies the SS-model-dependent computations of MB Kalman filtering, replacing them with a dedicated RNN operating on specific features encapsulating the information needed for its operation. Doing so enables KalmanNet to carry out real-time state estimation in the same manner as the KF (and EKF), while learning to overcome model mismatches and non-linearities. KalmanNet uses a relatively compact RNN, that can be trained with a relatively small data set, and infers a reduced complexity, making it applicable for high dimensional SS models and computationally limited devices.

ACKNOWLEDGEMENT

We would like to thank Prof. Hans-Andrea Loeliger for his helpful comments and discussions, and Jonas Mehr for his assistance with the numerical study.

REFERENCES

- [1] G. Revach, N. Shlezinger, R. J. G. van Sloun, and Y. C. Eldar, "KalmanNet: Data-driven Kalman filtering," in *Proc. IEEE ICASSP*, 2021, pp. 3905–3909.
- [2] R. E. Kalman, "A new approach to linear filtering and prediction problems," *Journal of Basic Engineering*, vol. 82, no. 1, pp. 35–45, 1960.
- [3] R. E. Kalman and R. S. Bucy, "New results in linear filtering and prediction theory," 1961.
- [4] R. E. Kalman, "New methods in Wiener filtering theory," 1963.
- [5] M. Gruber, "An approach to target tracking," MIT Lexington Lincoln Lab, Tech. Rep., 1967.
- [6] R. E. Larson, R. M. Dressler, and R. S. Ratner, "Application of the extended kalman filter to ballistic trajectory estimation," Stanford Research Institute, Tech. Rep., 1967.
- [7] J. D. McLean, S. F. Schmidt, and L. A. McGee, *Optimal filtering and linear prediction applied to a midcourse navigation system for the circumlunar mission*. National Aeronautics and Space Administration, 1962.
- [8] F. Auger, M. Hilairet, J. M. Guerrero, E. Monmasson, T. Orlowska-Kowalska, and S. Katsura, "Industrial applications of the Kalman filter: A review," *IEEE Trans. Ind. Electron.*, vol. 60, no. 12, pp. 5458–5471, 2013.
- [9] S. J. Julier and J. K. Uhlmann, "New extension of the Kalman filter to nonlinear systems," in *Signal Processing, Sensor Fusion, and Target Recognition VI*, vol. 3068. International Society for Optics and Photonics, 1997, pp. 182–193.
- [10] E. A. Wan and R. Van Der Merwe, "The unscented Kalman filter for nonlinear estimation," in *Proceedings of the IEEE Adaptive Systems for Signal Processing, Communications, and Control Symposium (Cat. No. 00EX373)*, 2000, pp. 153–158.
- [11] Y. LeCun, Y. Bengio, and G. Hinton, "Deep learning," *Nature*, vol. 521, no. 7553, p. 436, 2015.
- [12] Y. Bengio, "Learning deep architectures for AI," *Foundations and Trends® in Machine Learning*, vol. 2, no. 1, pp. 1–127, 2009.
- [13] S. Hochreiter and J. Schmidhuber, "Long short-term memory," *Neural computation*, vol. 9, no. 8, pp. 1735–1780, 1997.
- [14] J. Chung, C. Gulcehre, K. Cho, and Y. Bengio, "Empirical evaluation of gated recurrent neural networks on sequence modeling," *preprint arXiv:1412.3555*, 2014.
- [15] A. Vaswani, N. Shazeer, N. Parmar, J. Uszkoreit, L. Jones, A. N. Gomez, L. Kaiser, and I. Polosukhin, "Attention is all you need," *arXiv preprint arXiv:1706.03762*, 2017.
- [16] M. Zaheer, A. Ahmed, and A. J. Smola, "Latent LSTM allocation: Joint clustering and non-linear dynamic modeling of sequence data," in *International Conference on Machine Learning*, 2017, pp. 3967–3976.
- [17] N. Shlezinger, N. Farsad, Y. C. Eldar, and A. J. Goldsmith, "ViterbiNet: A deep learning based Viterbi algorithm for symbol detection," *IEEE Trans. Wireless Commun.*, vol. 19, no. 5, pp. 3319–3331, 2020.

- [18] N. Shlezinger, R. Fu, and Y. C. Eldar, "DeepSIC: Deep soft interference cancellation for multiuser MIMO detection," *IEEE Trans. Wireless Commun.*, vol. 20, no. 2, pp. 1349–1362, 2021.
- [19] N. Shlezinger, N. Farsad, Y. C. Eldar, and A. J. Goldsmith, "Learned factor graphs for inference from stationary time sequences," *arXiv preprint arXiv:2006.03258*, 2020.
- [20] N. Shlezinger, J. Whang, Y. C. Eldar, and A. G. Dimakis, "Model-based deep learning," *arXiv preprint arXiv:2012.08405*, 2020.
- [21] N. Carlevaris-Bianco, A. K. Ushani, and R. M. Eustice, "University of Michigan North Campus long-term vision and lidar dataset," *The International Journal of Robotics Research*, vol. 35, no. 9, pp. 1023–1035, 2016.
- [22] S. S. Haykin, *Adaptive filter theory*. Pearson Education India, 2014.
- [23] I. Arasaratnam, S. Haykin, and R. J. Elliott, "Discrete-time nonlinear filtering algorithms using Gauss–Hermite quadrature," *Proc. IEEE*, vol. 95, no. 5, pp. 953–977, 2007.
- [24] I. Arasaratnam and S. Haykin, "Cubature Kalman filters," *IEEE Trans. Autom. Control*, vol. 54, no. 6, pp. 1254–1269, 2009.
- [25] M. S. Arulampalam, S. Maskell, N. Gordon, and T. Clapp, "A tutorial on particle filters for online nonlinear/non-Gaussian Bayesian tracking," *IEEE Trans. Signal Process.*, vol. 50, no. 2, pp. 174–188, 2002.
- [26] J. Elfring, E. Torta, and R. van de Molengraft, "Particle filters: A hands-on tutorial," *Sensors*, vol. 21, no. 2, p. 438, 2021.
- [27] R. G. Krishnan, U. Shalit, and D. Sontag, "Deep Kalman filters," *preprint arXiv:1511.05121*, 2015.
- [28] M. Karl, M. Soelch, J. Bayer, and P. Van der Smagt, "Deep variational Bayes filters: Unsupervised learning of state space models from raw data," *preprint arXiv:1605.06432*, 2016.
- [29] M. Fraccaro, S. D. Kamronn, U. Paquet, and O. Winther, "A disentangled recognition and nonlinear dynamics model for unsupervised learning," in *Advances in Neural Information Processing Systems*, 2017.
- [30] C. Naesseth, S. Linderman, R. Ranganath, and D. Blei, "Variational sequential Monte Carlo," in *International Conference on Artificial Intelligence and Statistics*. PMLR, 2018, pp. 968–977.
- [31] E. Archer, I. M. Park, L. Buesing, J. Cunningham, and L. Paninski, "Black box variational inference for state space models," *arXiv preprint arXiv:1511.07367*, 2015.
- [32] R. Krishnan, U. Shalit, and D. Sontag, "Structured inference networks for nonlinear state space models," in *Proceedings of the AAAI Conference on Artificial Intelligence*, vol. 31, no. 1, 2017.
- [33] P. Abbeel, A. Coates, M. Montemerlo, A. Y. Ng, and S. Thrun, "Discriminative training of Kalman filters," in *Robotics: Science and Systems*, vol. 2, 2005, p. 1.
- [34] S. S. Rangapuram, M. W. Seeger, J. Gasthaus, L. Stella, Y. Wang, and T. Januschowski, "Deep state space models for time series forecasting," in *Advances in Neural Information Processing Systems*, 2018, pp. 7785–7794.
- [35] B. Laufer-Goldshtein, R. Talmon, and S. Gannot, "A hybrid approach for speaker tracking based on TDOA and data-driven models," *IEEE/ACM Trans. Audio, Speech, Language Process.*, vol. 26, no. 4, pp. 725–735, 2018.
- [36] L. Xu and R. Niu, "EKFNNet: Learning system noise statistics from measurement data," in *Proc. IEEE ICASSP*, 2021, pp. 4560–4564.
- [37] T. Haarnoja, A. Ajay, S. Levine, and P. Abbeel, "Backprop kf: Learning discriminative deterministic state estimators," in *Advances in Neural Information Processing Systems*, 2016, pp. 4376–4384.
- [38] X. Zheng, M. Zaheer, A. Ahmed, Y. Wang, E. P. Xing, and A. J. Smola, "State space LSTM models with particle MCMC inference," *preprint arXiv:1711.11179*, 2017.
- [39] H. Coskun, F. Achilles, R. DiPietro, N. Navab, and F. Tombari, "Long short-term memory Kalman filters: Recurrent neural estimators for pose regularization," in *Proceedings of the IEEE International Conference on Computer Vision*, 2017, pp. 5524–5532.
- [40] P. Becker, H. Pandya, G. Gebhardt, C. Zhao, C. J. Taylor, and G. Neumann, "Recurrent Kalman networks: Factorized inference in high-dimensional deep feature spaces," in *International Conference on Machine Learning*. PMLR, 2019, pp. 544–552.
- [41] L. Zhou, Z. Luo, T. Shen, J. Zhang, M. Zhen, Y. Yao, T. Fang, and L. Quan, "KFNet: Learning temporal camera relocalization using Kalman filtering," in *Proceedings of the IEEE/CVF Conference on Computer Vision and Pattern Recognition*, 2020, pp. 4919–4928.
- [42] V. G. Satorras, Z. Akata, and M. Welling, "Combining generative and discriminative models for hybrid inference," in *Advances in Neural Information Processing Systems*, 2019, pp. 13 802–13 812.
- [43] R. Dey and F. M. Salem, "Gate-variants of gated recurrent unit (GRU) neural networks," in *Proc. IEEE MWSCAS*, 2017, pp. 1597–1600.
- [44] P. J. Werbos, "Backpropagation through time: what it does and how to do it," *Proc. IEEE*, vol. 78, no. 10, pp. 1550–1560, 1990.
- [45] I. Sutskever, *Training recurrent neural networks*. University of Toronto Toronto, Canada, 2013.
- [46] A. López Escoriza, G. Revach, N. Shlezinger, and R. J. G. van Sloun, "Data-driven Kalman-based velocity estimation for autonomous racing," in *Proc. IEEE ICAS*, 2021.
- [47] D. P. Kingma and J. Ba, "Adam: A method for stochastic optimization," *preprint arXiv:1412.6980*, 2014.
- [48] Y. Bar-Shalom, X. R. Li, and T. Kirubarajan, *Estimation with applications to tracking and navigation: theory algorithms and software*. John Wiley & Sons, 2004.